Tunnelling and Underground Space Technology 95 (2020) 103140

Contents lists available at ScienceDirect

Tunnelling and Underground Space Technology

journal homepage: www.elsevier.com/locate/tust

Pressure-induced dipole theory and pressure pulsation in shallow urban road tunnels with top vents

Sike Jin[a,b,*], Jiali Jin[a], Yanfeng Gong[c]

[a] Architecture & Civil Engineering College, TVTC, Taizhou, PR China
[b] Green & Intelligent Building Research Center, TVTC, Taizhou, PR China
[c] Nanjing Tech University, Nanjing, PR China

ARTICLE INFO

Keywords:
Tunnel
Top vent
Pressure-induced dipole
Pulsation

ABSTRACT

Shallow urban road tunnels with top vents represent environmentally friendly and energy-saving technology. To date, four such tunnels are operational in Nanjing, and their intra-tunnel air quality has been widely acclaimed. However, no prescriptive design methods have been developed for this technology. Natural ventilation at the top of the tunnels is caused by the pressure difference inside and outside the top vents. Thus, a prerequisite to the development of scientific design methods for such tunnels is a complete understanding and representation of the pressure wave distribution pattern in the tunnels. Based on an analogy with an electric dipole, we propose a pressure-induced dipole theory and construct an intra-tunnel pressure distribution model. An experimental platform is developed to evaluate the pressure distribution inside tunnels under 6 operational conditions. The results suggest the following. (1) The proposed pressure-induced dipole theory can well describe and explain the pressure wave distribution rules in road tunnels. (2) With a uniform and continuous traffic flow, the real-time pressure on each point in the tunnels demonstrates periodical asymmetrical quasi-sinusoidal pulsation, where the cycle is given as $T = (S + L)/v$. (3) Periodical pressure pulsation with decaying amplitude exists around the top vents. With large top vents, the pressure exchange between the inside and outside of the tunnels is significant.

1. Introduction

Natural ventilation in shallow road tunnels with top vents is a green energy-saving technology that uses traffic wind produced by moving vehicles to guarantee a safe air environment relative to exhaust discharge in the tunnels. Such top vent systems significantly reduce draught fan operation costs. This technology has been successfully applied in several Chinese cities, such as the Hongxing Road tunnel (800 m) in Chengdu, Sichuan and the Tongjimen (890 m), Xianmen (1410 m) and Xinmofan Road (3000 m) tunnels in Nanjing, Jiangsu. The air quality in these tunnels has been widely acclaimed. However, the design and construction of such tunnels lack sufficient theoretical basis and experimental support, and the top vent ventilation mechanism has not been investigated systematically. Furthermore, this type of urban road tunnel does not comply with the *Specifications for Design of Ventilation and Lighting of Highway Tunnel* (JTJ026.1-1999). According to these specifications, mechanical ventilation should be adopted when the product of tunnel length and traffic flow in a one-way traffic tunnel is higher than 2000 (km × cars/h). Modic (2003a,b) stated that natural ventilation can be used in one-way tunnels shorter than 3000 m when the traffic flow is less than 750 cars/h in each lane and the vehicle running speed is greater than 30 km/h. However, this only applies to tunnels without top vents. Note that the current regulations do not consider top vents appropriate for tunnel ventilation.

Based on several studies of Zhong (2006), Wong et al. (2006), Palazzi et al. (2005), Ingason and Wickström (2006), Bogdan et al. (2008) and Tong et al. (2009), Jiangsu Province enacted the *Specifications for Design and Acceptance of Vertical Shaft Natural Ventilation in Urban Tunnels*(DGJ32/TJ102-2010). According to the specifications, vertical shafts should be distributed at a uniform spacing of 240 m or below; and when the tunnel length is in the range of 500–1500 m, the opening rate (effective opening area of vertical shaft/horizontal projected area of tunnel) should be no lower than 3.25%. However, no mature method with sufficient data support exists for the design of top vent locations in such tunnels. In addition, local construction authorities and fire brigades have expressed concern about such tunnels.

Therefore, academics and engineers have studied tunnels with top vents extensively. Yoon et al. (2006) from Inha University in Korea

* Corresponding author at: Architecture & Civil Engineering College, Institute of Green and Intelligent Building Research Center, PR China.
E-mail address: fallice2008@163.com (S. Jin).

https://doi.org/10.1016/j.tust.2019.103140
Received 30 January 2019; Received in revised form 30 August 2019; Accepted 6 October 2019
Available online 15 October 2019

Nomenclature

v	vehicle speed (m/s)
L	vehicle length (m)
S	vehicle spacing (m)
ρ	intra-tunnel air density (kg/m^3)
P_A	maximum positive pressure at the front of the vehicle (Pa)
P_B	maximum negative pressure at the rear of the vehicle (Pa)
A	positive polar distance (m)
B	negative polar distance (m)
C	distance from centre of top opening (m)
i	vehicle number
j	top opening number
x_i, y_i, z_i	coordinates of the front of vehicle i
x_j, y_j, z_j	coordinates of the centre of top opening j
F_j	area of top opening j (m^2)
K	spatial pressure distribution coefficient determined by the fluid media in tested space
α	tunnel pressure correction factor ($\alpha = 0.8$)
β	top opening pressure decay coefficient ($\beta = 0.17$)

employed a thermo-motive approach to compute the natural ventilation pressure of a long and wide tunnel in winter and summer. The results indicated that shaft height and temperature differences inside and outside the tunnel affected the natural ventilation pressure of the shafts. However, most subsequent study, found thermal pressure to be the major factor of natural ventilation only when there is a traffic jam. Under normal traffic conditions, thermal pressure can be ignored because the air pressure produced by vehicles is far greater than the thermal pressure, according to the studies of Yang (2007), Zhong et al. (2008), Bari and Naser (2010). Zhong et al. (2006) investigated the ventilation mechanism of such tunnels under the assumption that the traffic flow in random motion in the tunnels is constant and continuous and the intra-tunnel flow field is a one-dimensional pipe flow. According to their results, the air resulting from moving vehicles in a one-way road tunnel with multiple vents formed a concussive pressure pulsation at the vents such that the air inside and outside the tunnel could be exchanged. On this basis, they developed formulas to compute the air pressure in the tunnel, as well as the air input and output at the top vents. However, relative to the flow field within road tunnels, the correctness of the tube flow assumption is disputed. Most of these conclusions have not been verified experimentally or vary significantly from existing experimental data. Based on simplified flow filed in the buried section and Prandtl velocity distribution law, Jin et al. (2015) presented the formula of velocity distribution in the buried section, and energy transfer and dissipation law in the tunnel flow field were explained. Also, Jin et al. (2017) tested the distribution of air velocities and the flow-field characteristics, the results show that 1. At a constant vehicle flow, the airflow at the roof opening was always from outside to inside, and no respiration phenomenon was observed. 2. The maximum inlet velocity was at openings near the tunnel entrance, and the velocity gradually decreased as the openings were placed deeper into the tunnel. The inlet velocity exhibited a concave curve along the tunnel length.

Although previous studies have failedto explainthe mechanism of natural top vent ventilation in shallowtunnels, they all confirm that traffic air resulting from moving vehicles forms oscillating pressure pulsation at the vents so that repeated air exchange is established between the inside environment of tunnel and the outside atmosphere. Naturalventilation at the top of tunnels is driven by thepressure difference inside and outside the top vents;thus,the pressure pulsation within road tunnels can affect natural ventilation at top vents. Consequently, the following questions must be addressedto develop scientific design approaches for such tunnels.1. What rule does the pressure pulsation follow within aroad tunnel?2. How dotop vents affectpressure distribution within the tunnel?3. Can aregular expression of pressure pulsation within the tunnelsbe derived?In light of thesequestions, this paper proposes apressure-induced dipole theory and constructsa pressure distribution model for road tunnels. In addition, a 1/10-scale testing platform forroad tunnel ventilation is developedto test the pressure distribution within the tunnels underdifferent operationalconditions, verify the proposedtheory and find answers to the abovementioned questions.

2. Pressure-induced dipole theory

2.1. Single-point pressure field in tunnel space

For a running vehicle, the airflow velocity around the head is always less than the vehicle's speed. Therefore, a positive pressure zone is formed when the vehicle contacts the air in front of the vehicle. In contrast, at the rear of the vehicle, the air flow swirls due to the stripping phenomenon to form a negative pressure zone, according to the studies of Cooper and Campbell (1981), Chen et al. (1998), Tong et al. (2014) and Wang et al. (2011, 2014). Moreover, a single positive pressure point and a single negative point occur at the front and rear of each vehicle, respectively. The front positive pressure and rear negative pressure appear simultaneously and decay gradually. The combined effect of multiple vehicles will result in different levels of intermittent pressure pulsations in a tunnel.

The following hypotheses are proposed to simplify the question and realise a pressure wave equation.

(1) The air in the highway tunnel is at room temperature and atmospheric pressure. Air flow triggered by vehicle running inside the tunnel is low-speed flow with the Mach number (M) less than 0.3. So the air in the tunnel is assumed to be isotropic ideal gas with constant temperature.
(2) The viscosity of the air is small. Also, the impact of viscosity on the flow is restricted to the boundary layer near the wall. So the flow outside the boundary layer can be processed as an ideal fluid. In addition, the turbulence in the tunnel is highly intensive due to the perturbation of running vehicles, and the boundary layer near the wall is thin. Therefore, it's reasonable to assume that no viscosity exists in the air in this study.
(3) When pressure waves propagate in the fluid medium, the viscosity of the medium is the main cause of energy attenuation. Since the absence of viscosity in the air is assumed, there is no energy loss in the pressure wave propagation. Specifically, this assumption is a ratiocination of the third assumption.
(4) The pressure wave in the tunnel with low value and high frequency is propagated through sound velocity at a fast speed. As a result, the density of the gas changes quickly with a narrow range. Meanwhile, energy exchange caused by thermal conduction is very little. The pressure wave propagating in the air can be deemed as an adiabatic process.

An air microelement $\mathrm{d}V$ is selected from the pressure field of the tunnel (Fig.1), where $\mathrm{d}V = \mathrm{d}x\mathrm{d}y\mathrm{d}z$. In a tunnel, pressure p varies with the spatial location; therefore, the pressure on different surfaces of the air microelement is non-equivalent. Moreover, the air microelement is sufficiently small such that the pressure acting on its surfaces is uniform. Here, consider the force along the x direction. Assume the pressure intensity on the left surface of air microelement is $p_x = p$. Then, the force on this surface is given as $F_x = p_x\mathrm{d}y\mathrm{d}z = p\mathrm{d}y\mathrm{d}z$. In addition, assume the pressure intensity on the right surface of the air microelement is $p'_x = p + \mathrm{d}p$. Then, the force on the right surface is given as

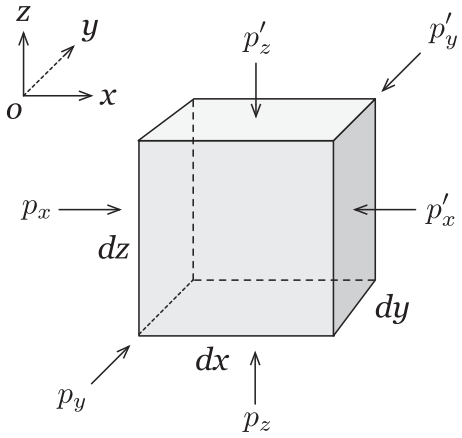

Fig. 1. Air microelement in pressure field.

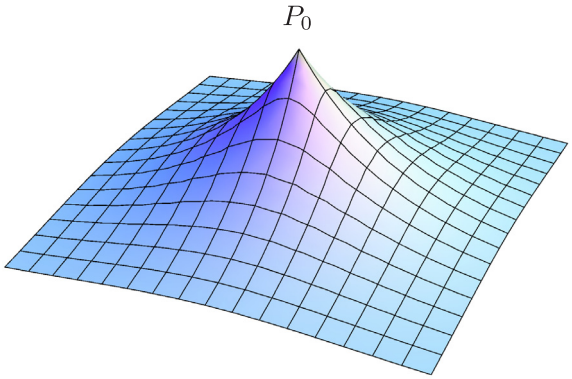

Fig. 2. Pressure distribution theory for isotropic fluid in infinite space.

$F'_x = p'x\mathrm{d}y\mathrm{d}z = (p + \mathrm{d}p)\mathrm{d}y\mathrm{d}z$. The composite force imposed on this microelement in the x direction is expressed as follows.

$$F = F_x - F'_x = \mathrm{d}p\mathrm{d}y\mathrm{d}z = \frac{\partial p}{\partial x}\mathrm{d}x\mathrm{d}y\mathrm{d}z \tag{1}$$

Suppose the air density ρ is a constant. Then, the mass of the microelement is given as $\mathrm{d}m = \rho\mathrm{d}x\mathrm{d}y\mathrm{d}z$. The composite force on the microelement is non-zero; therefore, the microelement will accelerate in the x direction (i.e. $\mathrm{d}u_x/\mathrm{d}t$).

The following can be inferred according to Newtons Second Law.

$$\frac{\partial p}{\partial x}\mathrm{d}x\mathrm{d}y\mathrm{d}z = \rho\mathrm{d}x\mathrm{d}y\mathrm{d}z\frac{\mathrm{d}u_x}{\mathrm{d}t} \tag{2}$$

Further collation yields the following.

$$\frac{\partial p}{\partial x} = \rho\frac{\mathrm{d}u_x}{\mathrm{d}t} \tag{3}$$

$$\frac{\mathrm{d}u_x}{\mathrm{d}t} = \frac{\partial u_x}{\partial t} + u_x\frac{\partial u_x}{\partial x} + u_y\frac{\partial u_x}{\partial y} + u_z\frac{\partial u_x}{\partial z} \tag{4}$$

Similarly, the motion equations in the y and z directions are given as follows.

$$\frac{\partial p}{\partial y} = \rho\frac{\mathrm{d}u_y}{\mathrm{d}t} \tag{5}$$

$$\frac{\partial p}{\partial z} = \rho\frac{\mathrm{d}u_z}{\mathrm{d}t} \tag{6}$$

$$\frac{\mathrm{d}u_y}{\mathrm{d}t} = \frac{\partial u_y}{\partial t} + u_x\frac{\partial u_y}{\partial x} + u_y\frac{\partial u_y}{\partial y} + u_z\frac{\partial u_y}{\partial z} \tag{7}$$

$$\frac{\mathrm{d}u_z}{\mathrm{d}t} = \frac{\partial u_z}{\partial t} + u_x\frac{\partial u_z}{\partial x} + u_y\frac{\partial u_z}{\partial y} + u_z\frac{\partial u_z}{\partial z} \tag{8}$$

The motion equation of the pressure wave is derived by combining Eqs. (3)–(8) as follows.

$$\rho\left[\frac{\partial \mathbf{V}}{\partial t} + (\mathbf{V}\cdot\nabla)\mathbf{V}\right] + \nabla p = 0 \tag{9}$$

$$\mathbf{V}\cdot\nabla = u\frac{\partial}{\partial x} + v\frac{\partial}{\partial y} + w\frac{\partial}{\partial z} \tag{10}$$

$$\nabla p = \mathbf{i}\frac{\partial p}{\partial x} + \mathbf{j}\frac{\partial p}{\partial y} + \mathbf{k}\frac{\partial p}{\partial z} \tag{11}$$

In the following, we focus on the air microelement. In the x direction, assume the mass of fluid flowing into it from the left surface of the air microelement is $\rho u_x\mathrm{d}y\mathrm{d}z$, while that flowing out from the right surface is $[\rho u_x + \mathrm{d}(\rho u_x)]\mathrm{d}y\mathrm{d}z$. In addition, assume the mass increment in the microelement is $(\partial\rho/\partial t)\mathrm{d}x\mathrm{d}y\mathrm{d}z$. Thus, an equation of continuity can be formed as follows.

$$\frac{\partial \rho}{\partial t}\mathrm{d}x\mathrm{d}y\mathrm{d}z = \rho u_x\mathrm{d}y\mathrm{d}z - \left[\rho u_x + \frac{\partial(\rho u_x)}{\partial x}\mathrm{d}x\right]\mathrm{d}y\mathrm{d}z \tag{12}$$

Eq. (13) is derived from Eq. (12).

$$\frac{\partial \rho}{\partial t} + \frac{\partial}{\partial x}(\rho u_x) = 0 \tag{13}$$

To this point, the x direction involves three variables p, u_x and ρ. However, the number of equations is only two. Therefore, no solution can be obtained and a third equation is required.

This third equation can be derived according to the thermodynamic properties of air. When a pressure wave passes the air microelement, its physical parameters, e.g. pressure intensity, density and temperature, change according to the thermodynamic equations. Note that the air medium in the tunnel is assumed to be ideal; thus, the transmission speed of the pressure wave is sufficiently fast such that there is not enough time for internal volume compression or expansion of air. Therefore, due to the short time required to transmit a pressure wave, we consider that the air microelement does not exchange heat with its surrounding environment. Consequently, the pressure wave process can

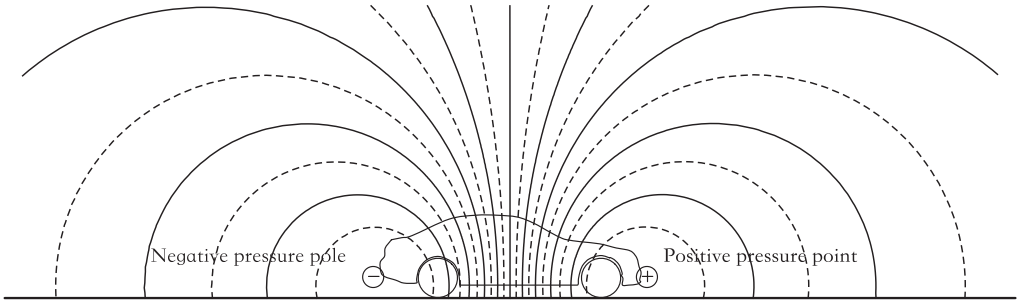

Fig. 3. Two-dimensional potential distribution of pressure dipole.

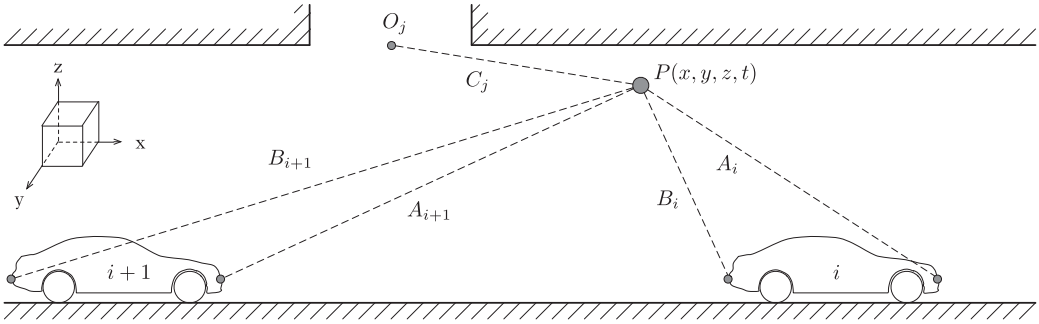

Fig. 4. Pressure distribution calculation.

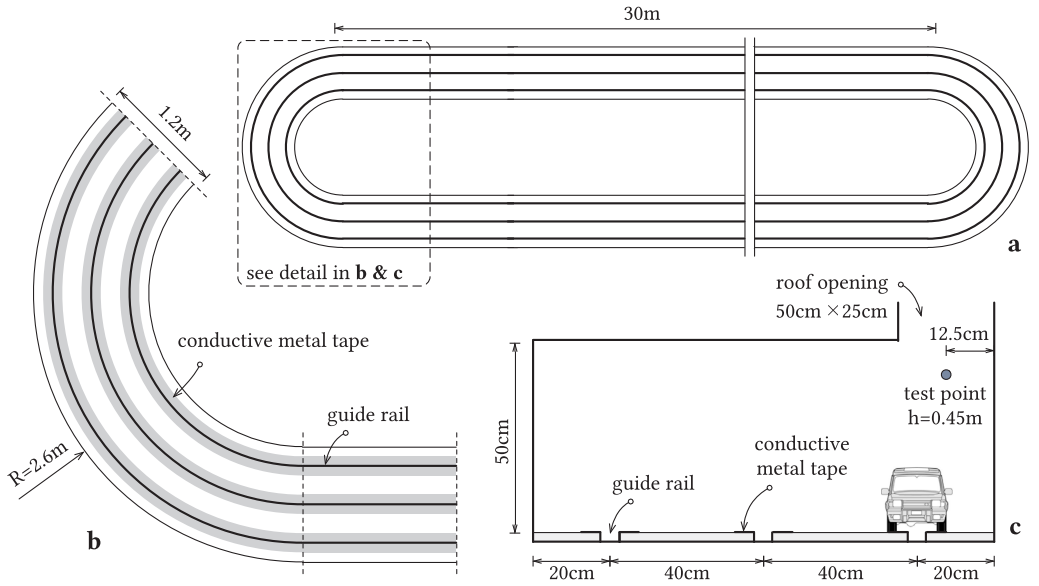

Fig. 5. Detail of model tunnel platform: (a) top view of the three-lane circular runway; (b) partial detail of the three-lane circular runway; (c) cross section of the model tunnel and the test points.

Fig. 6. Experimental platform.

be considered an adiabatic process. The adiabatic equation of ideal air is given as follows.

$$p\rho^{-\gamma} = Const \tag{14}$$

For general fluid media, pressure intensity is a function of density and temperature. Given the adiabatic condition, we can provide the following universal equation of state.

$$\mathrm{d}p = c^2\mathrm{d}\rho \tag{15}$$

Here, c is sound velocity in the medium, $\gamma = C_p/C_v$ is the ratio of the gas' specific heat at constant pressure to the specific heat at constant

Table 1
Test program for pressure distribution in road tunnel.

No.	vehicle speed (m/s)	vehicle distance (m)	D_1 (m)	D_2 (m)	roof opening
A-1	2	2	0.1	0.2	×
A-2	2	4	0.2	0.4	×
A-3	2	8	0.3	0.6	×
B-1	2	2	0.1	0.2	○
B-2	2	4	0.2	0.4	○
B-3	2	8	0.3	0.6	○

Note: ×: with no roof opening; ○: with roof opening on the top

temperature ($\gamma = 1.4$ for air).

The following pressure pulsation equation in macro space can be derived by combining Eq. (9), (13) and (15).

$$\frac{\partial^2 p}{\partial x^2} + \frac{\partial^2 p}{\partial y^2} + \frac{\partial^2 p}{\partial z^2} = \frac{1}{c^2}\frac{\partial^2 p}{\partial t^2} \tag{16}$$

Alternatively, we can also obtain the following.

$$\nabla^2 p = \frac{1}{c^2}\frac{\partial^2 p}{\partial t^2} \tag{17}$$

Typically, in an isotropous and free space medium, the pressure wave radiates in the form of a spherical wave. Here, a spherical coordinate system is selected, where the distance from the origin point of the pressure wave to the discussion point is denoted r. The pressure wave equation can be rewritten as follows.

$$\frac{\partial^2 p}{\partial r^2} + \frac{2}{r}\frac{\partial p}{\partial r} = \frac{1}{c^2}\frac{\partial^2 p}{\partial t^2} \tag{18}$$

Boundary conditions are introduced, and the pressure at the centre of the pressure wave achieves the highest value (i.e. P_0).

$$r = 0 \quad p = P_0 \tag{19}$$

At the place indefinitely far away from the center of pressure wave, relative pressure reaches the min value (i.e. $p = 0$). Therefore, we obtain the following.

$$r \to \infty \quad p = 0 \tag{20}$$

A universal solution to the pressure wave equation (Eq. (21)) in macro space can be obtained by substituting the boundary condition equations (Eq. (19) and (20)), into Eq. (18).

$$\frac{P_0}{p(r)} = \mathrm{Exp}(\omega t + \alpha r) + \mathrm{Exp}(\omega t - \alpha r) \tag{21}$$

Table 2
Mean standard deviation and mean measurement uncertainty (Pa).

Experiment No.	A-1	A-2	A-2	B-1	B-2	B-3
Standard deviation	0.073	0.082	0.066	0.085	0.085	0.097
Measurement uncertainty	0.034	0.041	0.027	0.037	0.038	0.043

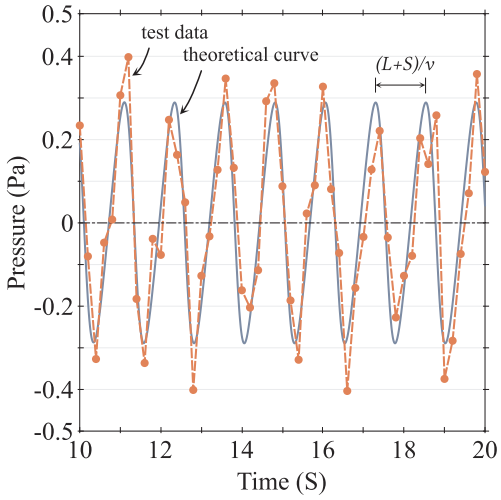

Fig. 8. Pressure pulsation at a fixed point (S = 2 m).

Here, r is the distance from the discussion point to the centre of the pressure wave, α is a to-be-determined constant (assumed as 0.8 in our experiment), ω is the angular frequency (assumed as 0 because the central air pressure remains constant when vehicles in the tunnel move at uniform speed). $\mathrm{Exp}(\omega t + \alpha r)$ is the incoming wave equation, and $\mathrm{Exp}(\omega t - \alpha r)$ is the reflected wave equation. The amplitude of the pressure pulsation in a road tunnel is low. In addition, the reflection coefficient of a concrete surface in a road tunnel against the air pressure wave is approximately 0.02. Thus, the reflected pressure wave in tunnels can be ignored.

Therefore, a point-source pressure wave equation applicable to road tunnels is derived as follows.

$$p(r) = \frac{P_0}{\mathrm{Exp}(\alpha r)} \tag{22}$$

$$r = \sqrt{(x - x_0)^2 + (y - y_0)^2 + (z - z_0)^2} \tag{23}$$

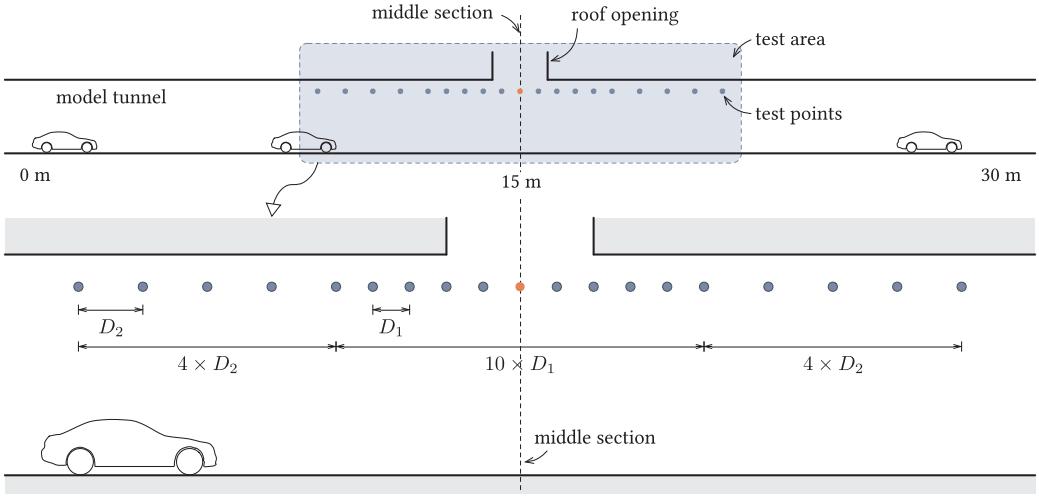

Fig. 7. Arrangement of test points for pressure distribution in road tunnel.

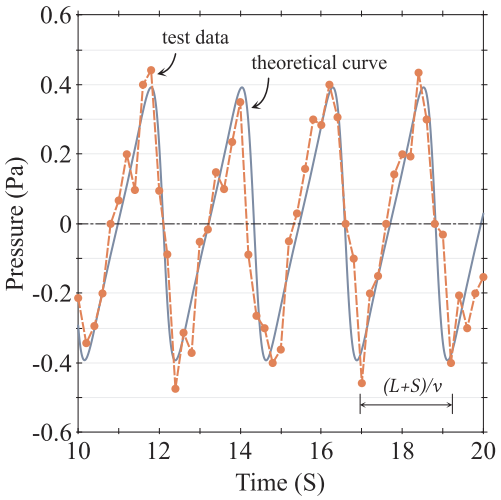

Fig. 9. Pressure pulsation at a fixed point (S = 4 m).

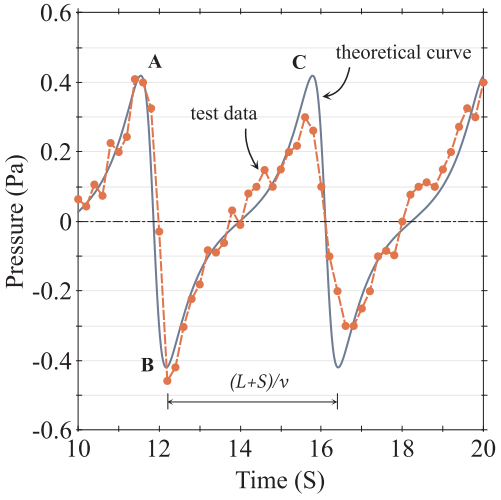

Fig. 10. Pressure pulsation at a fixed point (S = 8 m).

Here, (x, y, z) is the spatial coordinate of the discussion point and (x_0, y_0, z_0) is the coordinate of the centre of the pressure wave.

This equation is applicable to normal driving conditions since one of the assumptions deduced theoretically is that air in the tunnel is an isotropic ideal gas. Therefore, when a fire occurs in the tunnel, the calculated result will be quite different from the actual result. Fire may result in large temperature difference in the tunnel and a large amount of smoke, the physical properties of the smoke are significantly different from that of the air. At this point, stratified flows of smoke and air, or smoke particles will be formed and spread in the entire tunnel space, destroying the assumption of isotropic ideal gas.

According to the pressure wave spatial distribution equation (Eq. (22), (23)), an isolated pressure point in the space can form a pressure field with declining intensity around it. The pressure is P_0 at the centre of the pressure wave and 0 at infinity. A three-dimensional diagram is shown in Fig.2.

2.2. Pressure wave distribution model for running vehicles

The essence of establishing a pressure field in road tunnels lies in energy transmission and conversion. From a micro-perspective, moving vehicles collide with non-rigid air micro-masses in a non-elastic manner such that the air micro-masses have higher energy and speed that equals that of the vehicles. As a result, there is a shorter free path between the air micro-masses. In addition, the air micro-masses have higher density, potential energy and air pressure. At the point of collision, the dynamic energy of the air micro-masses is converted completely to potential energy. At this time, the air in front of the vehicles will theoretically gain the maximum positive pressure. In addition, as the vehicles keep running, the positive pressure at the front will maintain continuity. Here, the positive pressure is expressed as follows.

$$P_A = \frac{1}{2}\rho v_0^2 \tag{24}$$

Similarly, the maximum theoretical negative pressure at the rear of the vehicles is expressed as follows.

$$P_B = -\frac{1}{2}\rho v_0^2 \tag{25}$$

Here, ρ is air density and v_0 is vehicle velocity.

For each moving vehicle, one positive pressure point and one negative pressure point can always be formed in front and behind the vehicle. Moreover, the positive pressure in front and negative pressure at the rear appear simultaneously. Therefore, in this paper, the front positive pressure point is referred to as the positive pole of pressure, and the negative pressure point at the rear is referred to as the negative pole. A combination of these pressure points is considered a pressure dipole (Fig.3), and each running vehicle can be approximated as a pressure dipole.

The pressure field in space is a scalar quantity that can be superposed. Thus, the pressure of any point in the tunnel is equal to the superposed pressure fields (Fig.4 produced by all running vehicles (pressure dipoles). Under the composite effect of many running vehicles, the pressure distribution in the tunnel will be nonuniform. Here, we set the centre point of the road at the tunnel entrance as the null point of coordinates to erect a rectangular coordinate system. t is the running time, and the null point of time is the instant the traffic flow arrives at the tunnel entrance. Assume there are n vehicles in a part of the traffic flow. Thus, according to the pressure dipole theory, the dynamic pressure distribution model in road tunnels is expressed as follows.

$$P(x, y, z, t) = \sum_{i=1}^{n}\left[\frac{P_A}{Exp(\alpha A_i)} + \frac{P_B}{Exp(\alpha B_i)}\right] \tag{26}$$

$$A_i(x, y, z, t) = \sqrt{(x - x_i)^2 + (y - y_i)^2 + (z - z_i)^2} \tag{27}$$

$$B_i(x, y, z, t) = \sqrt{(x - x_i + L_i)^2 + (y - y_i)^2 + (z - z_i)^2} \tag{28}$$

Here, P_A and P_B are the pressures at the positive and negative poles in the pressure dipole. L_i is the length of vehicle i. A_i and B_i are the positive and negative polar distances of vehicle i at moment t, which are given by Eqs. (27) and (28). And x_i, y_i, z_i are the coordinates of the positive pole in front of vehicle i.

2.3. Road tunnel pressure wave distribution model with top vents

The entrance, exit and top vents of a tunnel directly connect the internal tunnel space to the outside, which affects the pressure distribution within the tunnel. Subsequent experimental results suggest that, affected by running vehicles, the intra-tunnel pressure displays time-dependent pulsation and varies at intervals along the tunnel length. Moreover, the positive and negative pressures accumulated in the tunnel are released at the entrance, exit and top vents, where pressure pulsation reveals decay. The vent size also affects the pressure releasing effect (i.e. a larger vent results in a wider influence area). At the centre of the top vents, the pressures inside and outside the vents are exchanged fully such that they are equal and the amplitude becomes zero. With increasing distance, the effect of the vents on the intra-tunnel pressure also declines.

In view of the above phenomena, this paper proposes the pressure decay function ζ. In the pressure distribution model for road tunnels

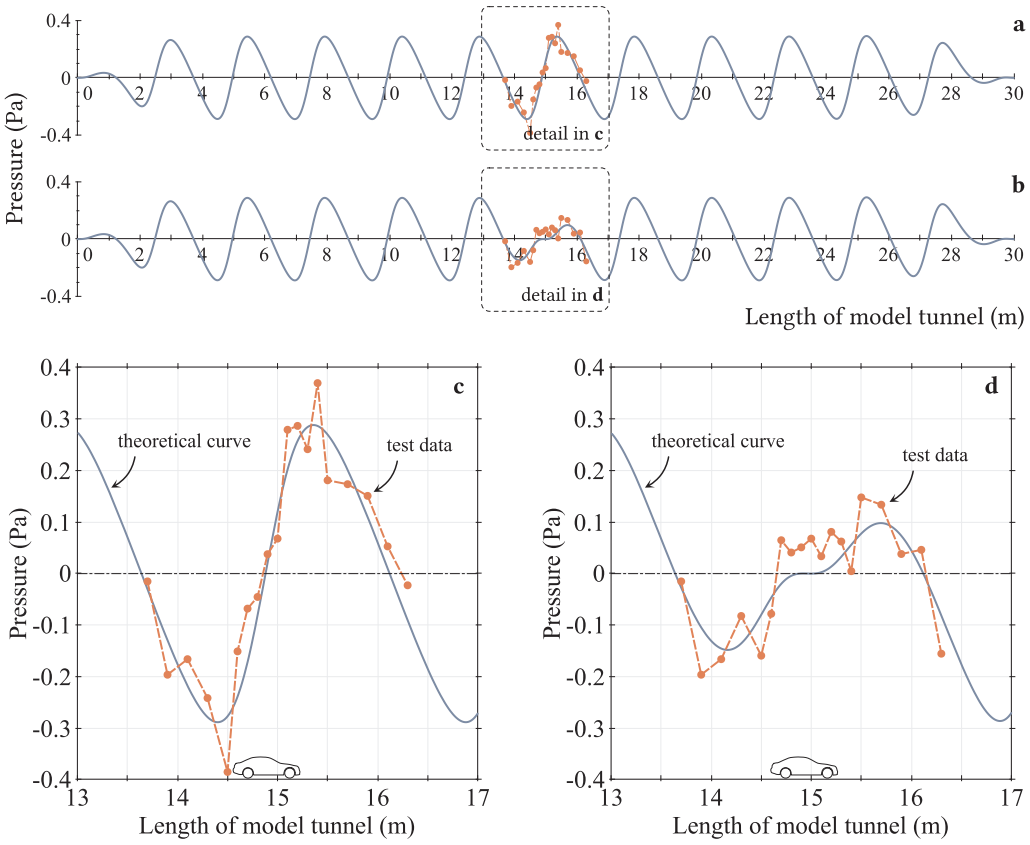

Fig. 11. Pressure distribution curve in tunnel (S = 2 m): (a) the intra-tunnel pressure distribution curve with no top vent; (b) the intra-tunnel pressure distribution curve with top vents; (c) details of the dotted boxes in subfigures a; (d) details of the dotted boxes in subfigures b.

with top vents, the effect of the entrance, exit and top vents on the intra-tunnel pressure distribution is corrected using the proposed pressure decay function ζ.

Here, assume the coordinate of the centre of vent j at the top is (x_j, y_j, z_j). Then, the pressure decay function ζ at the top vent is expressed as follows.

$$\zeta_j(x, y, z) = 1 - \frac{1}{\mathrm{Exp}(\beta C_j^2 / F_j)} \tag{29}$$

Here, β is a to-be-determined coefficient ($\beta = 0.17$ in this paper), F_j is the area of top vent j and C_j is the distance from the centre of top vent j to the computed point. C_j can be computed as follows.

$$C_j(x, y, z) = \sqrt{(x - x_j)^2 + (y - y_j)^2 + (z - z_j)^2} \tag{30}$$

Then, the pressure wave distribution in a road tunnel with top vents can be computed as follows.

$$P(x, y, z, t) = \prod_{j=1}^{m} \zeta_j \sum_{i=1}^{n} \left[\frac{P_A}{Exp(\alpha A_i)} + \frac{P_B}{Exp(\alpha B_i)} \right] \tag{31}$$

3. Model experiment

3.1. Experimental platform

We conducted a road tunnel experiment using a three-lane circular runway with 30 m straight sections on both sides and a total lane width of 1.2 m. The net height of the model tunnel was 0.5 m (Fig.5, 6). The model tunnel was paved with composite board and embedded with three tracks at an interval of 40 cm. Both sides of the tracks were pasted with a conductive metal strap to provide the model vehicles with a continuous power supply. Note that the vehicle speed could be adjusted by changing the voltage between the conductive metal straps. All joints in the tunnel model were well sealed. The top vents were 250 mm wide and 500 mm long, and were laid along the sides. On the top, a mobile transparent cover was fixed to adjust the vent length and adapt the model to test different conditions. The dimensions of the model vehicles were 480 mm × 250 mm × 200 mm. A micro-pressure transmitter (reaction time, 0.2 s) was used as the test instrument.

3.2. Test plan

This study incorporated 6 groups of tests according to top vent and vehicle spacing settings. The tests are described as follows.

Group 1–3 (A-1, A-2 and A-3): To eliminate the effect of the top vent on intra-tunnel pressure when the pressure pulsation pattern and distribution were tested in a buried section, there was no vent on the top of the tunnel in A-1, A-2 and A-3. To demonstrate the periodical pulsation rule of the pressure wave in the road tunnels, the vehicle spacing in Groups A-1, A-2 and A-3 was 2 m, 4 m and 8 m, respectively.

Group 4–6 (B-1, B-2 and B-3): In these groups, a single vent was positioned at the middle of the tunnel to rule out disturbance from other vents and test the pressure distribution features around the single top vent. This was expected to help determine the effect of a top vent on intra-tunnel pressure. Also, the vehicle spacing in Groups B-1, B-2 and B-3 was 2 m, 4 m and 8 m, respectively.

The vehicle speed was 2 m/s for each experimental condition. See Table 1 for the specific experimental parameters. The measurement points in each group were positioned as shown in Fig.7.

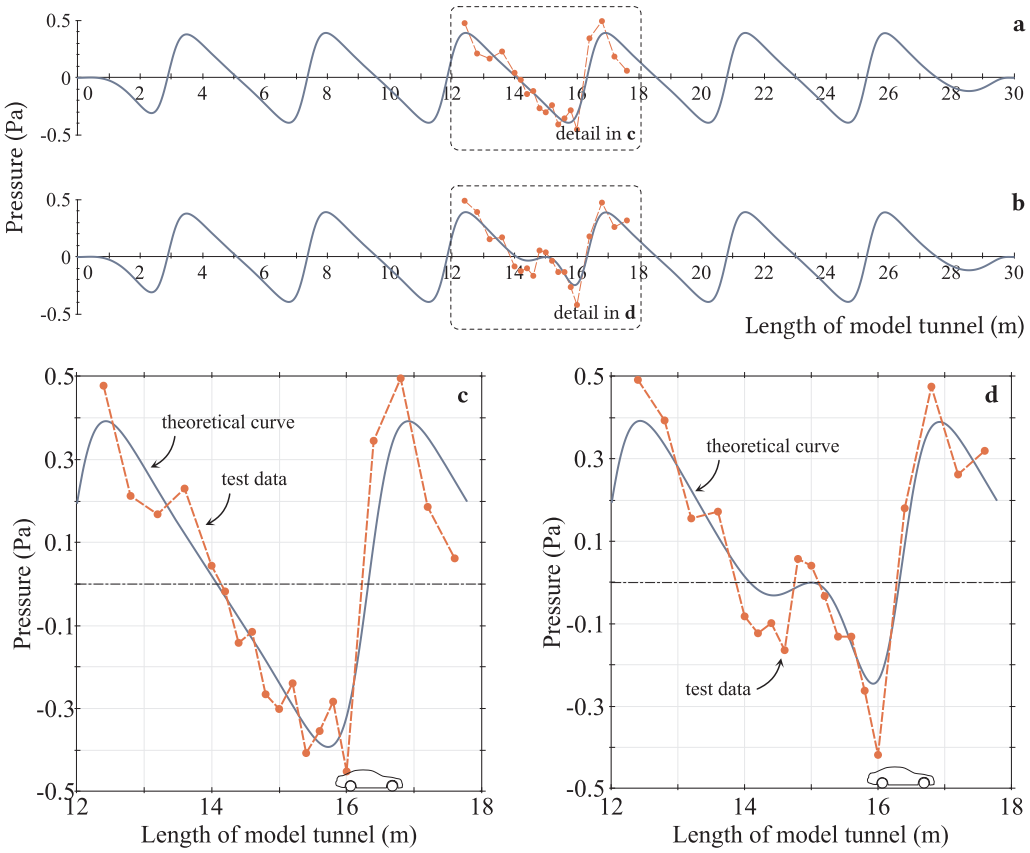

Fig. 12. Pressure distribution curve in tunnel (S = 4 m): (a) the intra-tunnel pressure distribution curve with no top vent; (b) the intra-tunnel pressure distribution curve with top vents; (c) details of the dotted boxes in subfigures a; (d) details of the dotted boxes in subfigures b.

4. Results and discussion

4.1. Data processing and error analysis

To reduce experimental error, each experimental condition was tested 5 times, and each data represent the average of the results. A class A evaluation was adopted to determine measurement uncertainty. An error analysis indicated that the total mean standard deviation of the test data was 0.081 Pa and the total measurement uncertainty was 0.037 Pa. As the size of the measurement data was quite large, the error and uncertainty of each measurement array was omitted. However, the error and uncertainty for each test group are shown in Table 2. In addition, according to the analysis, the measurement error for the tunnel with top vents was significantly higher than that without top vents. Despite high measurement error and uncertainty in some data, the general statistical outcome still well reflects the pressure distribution pattern in the tunnel.

4.2. Pressure pulsation within road tunnels

For a running vehicle, a positive pressure zone is formed when the front of the vehicle collides with the air. At the rear of the vehicle, air flow will swirl due to the stripping phenomenon to form a negative pressure zone. From a micro-perspective, a moving vehicle collides with non-rigid air micro-masses in a non-elastic manner such that the air micro-masses have the same speed as the vehicle. As a result, the air micro-masses have a shorter free path in between and higher air pressure.

Fig. 8–10 show the pressure pulsation of the central measuring points (marked in orange) between 10 and 20 s in experiments A-1, A-2 and A-3. Here, the solid blue line is the theoretical computation curve, and the orange dotted line indicates the test data. A comparison reveals that the theoretical computation result well matches the experimental data in most areas; however, greater errors appear around the peaks and troughs of the pressure pulsation, with a maximum relative error of 32.6%. Nevertheless, the pressure pulsation rules reflected by them are quite consistent with each other.

Both the theoretical computation and experimental test suggest that periodical pressure pulsation appears in road tunnels under the effect of moving vehicles. In each pulsation cycle, the pressure pulsation involves two stages.

In the first stage (i.e. A → B in Fig.10), the whole vehicle body passes below the measuring point. In this process, the pressure on this point rapidly falls from the peak to the Valley. In the second stage (i.e. B → C), the vehicle keeps running with the rear gradually leaving the measuring point. However, the next vehicle is approaching the measuring point; therefore, the pressure at this point gradually increases again to reach the peak.

Under a uniform traffic flow, the theoretical cycle of pressure pulsation in a road tunnel is given as follows.

$$T = \frac{S + L}{v} \tag{32}$$

Here, S is the vehicle length, L is vehicle spacing (m) and v is the vehicle velocity (m/s).

In this experiment, vehicle length is a constant value (0.48 m). When the vehicle spacing is 2 m, the theoretical cycle is 1.24 s. In contrast, the mean cycle from the experimental data is approximately 1.18 s. When the vehicle spacing is 4 m, the theoretical cycle is 4.24 s, and the mean cycle from the experimental data is approximately 4.20 s. Thus, the theoretical computation coincides well with the experimental data.

In a general traffic flow,vehicle spacing is far greaterthan the vehicle length; therefore,the duration of the first stage is significantly

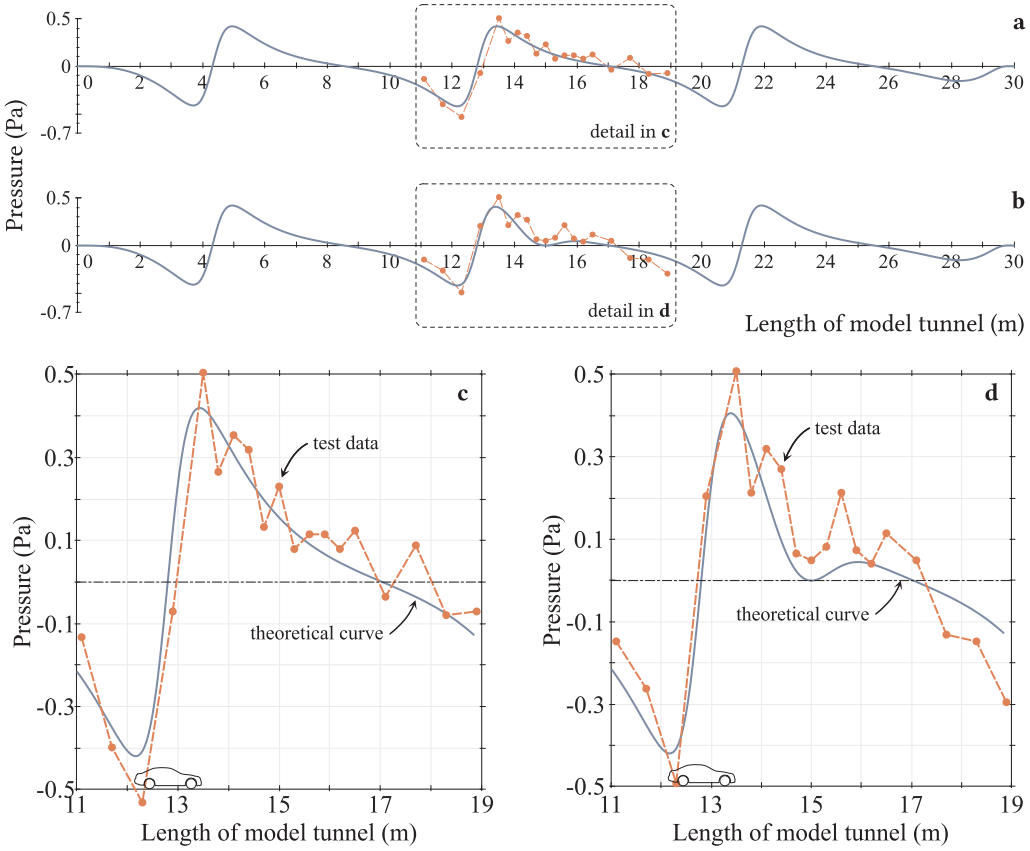

Fig. 13. Pressure distribution curve in tunnel (S = 8 m): (a) the intra-tunnel pressure distribution curve with no top vent; (b) the intra-tunnel pressure distribution curve with top vents; (c) details of the dotted boxes in subfigures a; (d) details of the dotted boxes in subfigures b.

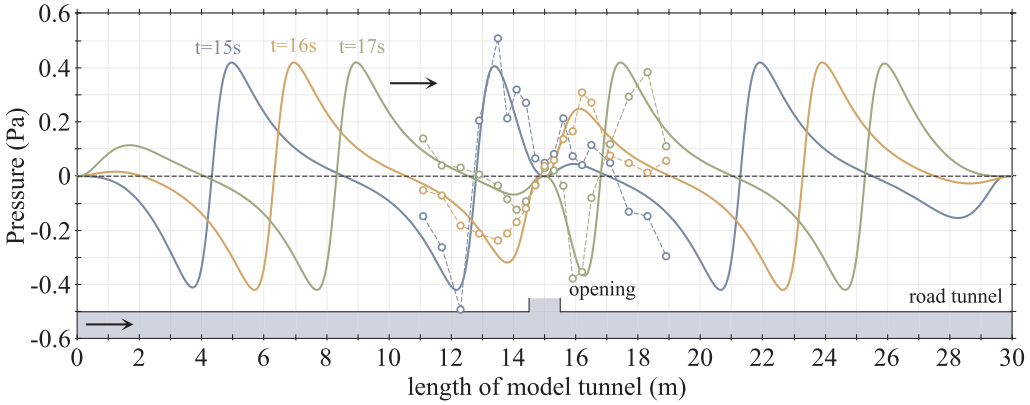

Fig. 14. Theoretical curves and experimental data for the intra-tunnel pressure distribution for experimental condition B-3.

lessthan that of the second stage in a singlepressure pulsation cycle. This is reflected by the rapid fall thengradual rise of the pressure shown in the figures. Therefore, the pressure pulsation in road tunnels manifests as an asymmetrical quasi-sinusoidal pulsation.

4.3. Pressure distribution in road tunnels

As suggested by the results, the pressure of different points in the road tunnels presents periodical pulsation under a continuous traffic flow. This section discusses the spatial distribution pattern of pressure in the road tunnels.

Figs. 11–13 illustrate the pressure distribution in road tunnels under different test plans for t = 15 s. Here, the solid blue line is the theoretical computation curve, and the orange dotted line indicates the test data. Due to a limitation in instrument quantity, 19 pressure measuring points were positioned at the middle section of the tunnel; therefore, they could not measure the pressure distribution throughout the entire tunnel. However, a local data comparison reveals that the theoretical curve is still highly consistent with the test data relative to the spatial distribution pattern of pressure.

The pressure of different points along the traffic flow in the tunnel also pulses periodically. When examining the figures at a certain moment, we find that a pressure wave peak appears around the front of each vehicle and a trough appears around the rear of the vehicle. As a result, under the composite effect of many vehicles, the pressure in road tunnels is distributed in a waveform. Under a uniform and continuous traffic flow, the theoretical wavelength of the pressure wave is given as follows.

$$S + L \tag{33}$$

Fig. 11–13, each contain four subfigures marked a, b, c and d, where subfigure a is the intra-tunnel pressure distribution curve with no top vent, subfigure b is the intra-tunnel pressure distribution curve with top vents and subfigures c and d show the details of the dotted boxes in subfigures a and b, respectively.

A comparison reveals that, in the presence of top vents, the pressure wave around the top vents declines in terms of amplitude because the positive pressure accumulated in front and negative pressure at the rear of the vehicle are released through the top vents when the vehicle is running. When the vehicle passes a top vent and enters the buried section again, the positive and negative pressures at the front and rear are accumulated again and released at the next top vent. This process continues in this manner.

The pressure decays more and gets released more radically when closer to the centre of the vent. When distant from the vent, the pressure is less affected by the vent in distribution. Pressure pulsation still exists near the top vents; however, it is not particularly significant due to the reduced amplitude. In addition, the cycle of the pressure pulsation near the top vents does not change, and it is the same as that of the pressure pulsation in the buried section.

Fig. 14 shows the theoretical curves and experimental data for the intra-tunnel pressure distribution for experimental condition B-3 when t is 15 s, 16 s and 17 s. As can be seen, the pressure wave in a road tunnel proceeds as the vehicle keeps running. As the time goes from t = 15s to t = 16s, the vehicle runs by 2 m, and the pressure wave also proceeds by 2 m in theory. According test data, the pressure wave advances by around 1.83 m within this period. Similarly, from t = 16 s to t = 17 s, the vehicle keeps running for another 2 m. It is suggested by the test data that, during this period, the pressure wave advances by 2.10 m. This means under uniform traffic flow, the speed of the pressure wave is equal to that of the vehicle.

5. Conclusion

For a running vehicle, a positive pressure zone is formed by the front of the vehicle colliding with the air, while, at the rear of the vehicle, the air flow will swirl due to the stripping phenomenon to form a negative pressure zone. Each running vehicle can form a positive and negative pressure point at the front and rear of the vehicle. The positive pressure point is a positive pressure pole, while that at the rear is a negative pressure pole (a combination of which is referred to as a pressure dipole). Each running vehicle can be approximated as a pressure dipole. The pressure at any point in the tunnel is the superposed pressure fields of all running vehicles (pressure dipoles) at the given point. The pressure dipole theory and dynamic pressure distribution model of a road tunnel can well describe and explain the pressure pulsation pattern and spatial distribution rules in road tunnels with top vents.

Affected by moving vehicles, the pressure at different points in road tunnels demonstrates a periodical pulsation phenomenon over time. In each pulsation cycle, the pressure pulsation involves two stages. In the first stage, the whole body of the vehicle passes underneath the measuring point. In this process, the pressure at this point rapidly falls from the peak to the trough. In the second stage, the vehicle moves beyond the measuring point; however, the next vehicle approaches the measuring point; thus, the pressure at this point gradually increases again to reach the peak. With a uniform and continuous traffic flow, the pressure pulsation cycle is (S + L)/v. The pulsation of pressure exists around top vents with the same cycle as that in a buried section but with a decaying amplitude.

Under the effect of running vehicles, the pressure of all points in the road tunnels also displays a periodical waveform distribution along the length. The peak of the pressure wave appears at the front of each vehicle, while the trough appears at the rear. With a uniform and continuous traffic flow, the pressure wave will have a theoretical wavelength of S + L. Furthermore, the pressure wave keeps advancing with the moving vehicles in a synchronous manner and their speeds are consistent.

Acknowledgment

The study was supported by Natural Science Foundation of Zhejiang Province of China (LQ18A02001) and 211 YoungTop-notchTalent Program of Taizhou (QBX1802009).

References

Bari, S., Naser, J., 2010. Simulation of airflow and pollution levels caused by severe traffic jam in a road tunnel. Tunn. Undergr. Space Technol. 25, 70–77. https://doi.org/10.1016/j.tust.2009.09.004. http://www.sciencedirect.com/science/article/pii/S0886779809000935.

Bogdan, S., Birgmajer, B., Kovačić, Z., 2008. Model predictive and fuzzy control of a road tunnel ventilation system. Transp. Res. Part C: Emerg. Technol. 16, 574–592. https://doi.org/10.1016/j.trc.2007.11.004. http://www.sciencedirect.com/science/article/pii/S0968090X07000897.

Chen, T., Lee, Y., Hstl, C., 1998. Investigations of piston-effect and jet fan-effect in model vehicle tunnels. J. Wind Eng. Ind. Aerodyn. 73, 99–110.

Cooper, K., Campbell, W., 1981. An examination of the effects of wind turbulence on the aerodynamic drag of vehicles. J. Wind Eng. Ind. Aerodyn. 9, 167–180. https://doi.org/10.1016/0167-6105(81)90087-8. http://www.sciencedirect.com/science/article/pii/0167610581900878.

Ingason, H., Wickström, U., 2006. The international forum of fire research directors: a position paper on future actions for improving road tunnel fire safety. Fire Saf. J. 41, 111–114. https://doi.org/10.1016/j.firesaf.2005.11.006. http://www.sciencedirect.com/science/article/pii/S0379711205001220.

Jin, S., Gong, Y., Zhang, G., 2015. Flow field development and energy evolution in road tunnels with unidirectional uniform traffic. J. Wind Eng. Ind. Aerodyn. 147, 66–76. https://doi.org/10.1016/j.jweia.2015.09.011. http://www.sciencedirect.com/science/article/pii/S0167610515002275.

Jin, S., Jin, J., Gong, Y., 2017. Natural ventilation of urban shallowly-buried road tunnels with roof openings. Tunn. Undergr. Space Technol. 63, 217–227. https://doi.org/10.1016/j.tust.2016.12.019. http://www.sciencedirect.com/science/article/pii/S0886779815303163.

Modic, J., 2003a. Air velocity and concentration of noxious substances in a naturally ventilated tunnel. Tunn. Undergr. Space Technol. 18, 405–410. https://doi.org/10.1016/S0886-7798(03)00044-0. http://www.sciencedirect.com/science/article/pii/S0886779803000440.

Modic, J., 2003b. Fire simulation in road tunnels. Tunn. Undergr. Space Technol. 18, 525–530. https://doi.org/10.1016/S0886-7798(03)00069-5. http://www.sciencedirect.com/science/article/pii/S0886779803000695.

Palazzi, E., Currò, F., Fabiano, B., 2005. A study on road tunnel fires using hazmat, with emphasis on critical ventilation velocity. Process Saf. Environ. Prot. 83, 443–451. https://doi.org/10.1205/psep.04214. http://www.sciencedirect.com/science/article/pii/S0957582005712799.

Tong, Y., MingHeng, S., YanFeng, G., JiaPeng, H., 2009. Full-scale experimental study on smoke flow in natural ventilation road tunnel fires with shafts. Tunn. Undergr. Space Technol. 24, 627–633. https://doi.org/10.1016/j.tust.2009.06.001. http://www.sciencedirect.com/science/article/pii/S0886779809000601.

Tong, Y., Wang, X., Zhai, J., Niu, X., Liu, L., 2014. Theoretical predictions and field measurements for potential natural ventilation in urban vehicular tunnels with roof openings. Build. Environ. 82, 450–458.

Wang, F., Wang, M., He, S., Deng, Y., 2011. Computational study of effects of traffic force on the ventilation in highway curved tunnels. Tunn. Undergr. Space Technol. 26, 481–489. https://doi.org/10.1016/j.tust.2011.01.003. http://www.sciencedirect.com/science/article/pii/S0886779811000150.

Wang, F., Wang, M., Wang, Q., Zhao, D., 2014. An improved model of traffic force based on cfd in a curved tunnel. Tunn. Undergr. Space Technol. 41, 120–126. https://doi.org/10.1016/j.tust.2013.12.006. http://www.sciencedirect.com/science/article/pii/S0886779813002113.

Wong, N.H., Song, J., Istiadji, A.D., 2006. A study of the effectiveness of mechanical ventilation systems of a hawker center in singapore using cfd simulations. Build. Environ. 41, 726–733.

Yang, Wu, 2007. Thermal environment measurement and research of high-density residential area in southern China — take Hong Kong, Shanghai and Guangzhou for example. Technical Report. Fifth National Architecture and Urban Planning Graduate Academic Forum.

Yoon, C.H., Kim, M.S., Kim, J., 2006. The evaluation of natural ventilation pressure in korean long road tunnels with vertical shafls. Tunn. Undergr. Space Technol.

Zhong, Gao, Gong, 2006. Discussion on natural ventilation action principle of traffc wind force. J. Railway Eng. Soc. 5 082–06.

Zhong, Gong, Tong, 2008. Similarity study on model experiment for natural ventilation in highway tunnels. HVAC 38, 13–16.

Zhong, Zeng, 2006. Distribution of harmful gas concentration in highway tunnel with natural ventilation. J. Railway Eng. Soc. 9 044–06.